

Research Article

Effect of Flexibility Ratio on Seismic Response of Cut-and-Cover Box Tunnel

Shamsher Sadiq ¹, Quang van Nguyen ¹, Hyunil Jung ¹ and Duhee Park ²

¹Graduate Student, Department of Civil and Environmental Engineering, Hanyang University, 222 Wangsimni-ro, Sageun-dong, Seongdong-gu, Seoul, Republic of Korea

²Professor, Department of Civil and Environmental Engineering, Hanyang University, 222 Wangsimni-ro, Sageun-dong, Seongdong-gu, Seoul, Republic of Korea

Correspondence should be addressed to Duhee Park; dpark@hanyang.ac.kr

Received 29 April 2019; Revised 14 June 2019; Accepted 14 July 2019; Published 29 July 2019

Academic Editor: Melina Bosco

Copyright © 2019 Shamsher Sadiq et al. This is an open access article distributed under the Creative Commons Attribution License, which permits unrestricted use, distribution, and reproduction in any medium, provided the original work is properly cited.

Equivalent linear time history analyses are conducted to calculate the seismic response of various types of cut-and-cover single box tunnels. A finite-element numerical model is calibrated against the results of centrifuge tests. The calculated tunnel responses compare favourably with the measurements. A validated model is then used to quantify the seismic response of box tunnels. The flexibility ratio (F) is illustrated to have a governing influence on the tunnel response. It is shown that the previously developed relationship between F and the racking ratio (R) is applicable for a wide range of F up to 20. It is also shown that an increase in F accompanies corresponding increase in R , the spectral acceleration in the tunnel lining, and the shear stress along the tunnel lining-soil interface. The thrust in the tunnel lining is also revealed to increase with F , although the calculated value is significantly lower than the pressure on yielding walls. Additionally, the surface settlement is shown to increase with an increase in F .

1. Introduction

Tunnels constitute an integral part of the transportation infrastructure in urban areas. Historically, tunnels have experienced a lower level of damage compared with above-ground structures during strong earthquakes. However, recent earthquakes have demonstrated that even tunnels are vulnerable to structural damage under severe excitation [1].

The seismic response of rectangular tunnels has been a subject of in-depth research. A wide range of studies using centrifuge tests [2–11], shaking table tests [12–19], and numerical simulations [7, 20–30] have been performed. Previous studies revealed that there is a unique relationship between flexibility ratio (F) and the racking ratio (R), where F is the relative stiffness between the tunnel and the surrounding soil and R is defined as the ratio of the displacement of the tunnel and free-field soil. Wang [31] used analytical equations to develop a correlation between F

and R for circular tunnels. A suite of linear dynamic analyses was performed for rectangular tunnels for which analytical solutions were not available in the guidelines of the National Cooperative Highway Research Program (NCHRP-611) [32]. An empirical F - R relationship that matches the F - R curves of Wang [31] was presented. It was reported to use the averaged strain-compatible equivalent linear (EQL) shear modulus to determine F to account for the soil nonlinearity.

The EQL analysis is widely used in seismic analysis of tunnels [4, 6], but the method has not yet been validated against recordings. In this study, a two-dimensional (2D) plane strain finite-element analysis was performed on a cut-and-cover tunnel using the EQL soil properties. The numerical model was calibrated against the centrifuge results of Gillis [9]. The effect of F on the pattern of the deformation shapes, distribution of mobilized shear stress along the tunnel lining, thrust in the lining, and corresponding surface settlement are investigated.

2. Numerical Model

A series of 2D dynamic analyses were performed using the finite-element (FE) analysis program ABAQUS [33]. The 2D plane strain computational model used in the analyses is shown in Figure 1. The numerical model simulates the centrifuge model test, details of which are presented in the following section. The numerical model is 104 m and 26 m in width and height, respectively. The tunnel is 14 m and 8 m in width and height, respectively.

A four-node plane strain element with reduced integration (CPE4R) and a two-node beam element (B21) were used to simulate the soil/rock and tunnel lining, respectively. The lateral boundaries of the computational domain were tied with a kinematic constraint to simulate the simple shear condition using the “multipoint constraints” (MPCs) option in ABAQUS. This technique creates periodic boundary conditions and is used to simulate the free-field condition of the soil deposits that extends infinitely in the horizontal direction. The lower boundary was fixed representing a rigid boundary. Slip and normal behaviour of the soil-structure interface was simulated using the surface-to-node interface. An interface slip coefficient was defined as $0.7 \tan(\varphi_{\text{soil}})$, as used by Deng et al. [34] and Zhang et al. [35] to validate the numerical model. Tsinidis [7] reported that simulating only the slip and restraining the potential separation between the soil and tunnel produces an unrealistic transmission of the tensile stress to the soil in contact. An interface element that allows potential normal separation between the tunnel lining and surrounding soil was used. The size of finite element was selected using the following equation, as recommended by Kuhlemeyer and Lysmer [36]:

$$\Delta l \leq \frac{\lambda}{10} \text{ to } \frac{\lambda}{8}, \quad (1)$$

where Δl is the size of the element and λ is the wavelength.

The nonlinearity of soil under seismic excitation plays an important role in the seismic response of tunnels. The EQL analyses have widely been used for the wave propagation in soil profiles excited by seismic loading. The EQL approach has also widely been adopted in seismic simulation of tunnels (e.g., [6] and [37]). The nonlinear analysis was reported to provide a better prediction of the seismic tunnel response, but the EQL analysis has been reported to provide a reasonable estimate [4, 5].

The EQL properties were determined via parallel one-dimensional (1D) nonlinear site response analysis performed using DEEPSOIL version 7.0 [38]. The non-Masing modulus reduction and damping curves fitting procedure, termed MRDF, was used to match the target nonlinear curves [39]. A generalized quadratic/hyperbolic (GQ/H) constitutive model [40] was used to apply the shear strength correction. The small strain damping was modelled with the Rayleigh damping formulation. The 1st and 5th modes were used to calculate the Rayleigh damping coefficients [41].

The process of extracting the EQL soil properties from DEEPSOIL and application to the 2D FEM time history analysis is shown in Figure 2. The effective shear strain

profile (defined as 0.65 of maximum shear strain) is calculated from DEEPSOIL, from which the corresponding shear modulus and damping ratio profiles are extracted. The extracted properties are applied to the FE model. 2D dynamic viscoelastic analysis is then performed. It should be noted that although the EQL approach has been reported to compare favourably with measurements, the residual between the nonlinear analysis may increase with an increase in the intensity of the ground motion. Therefore, it is recommended to use the nonlinear analysis for severe excitations where shear strain exceeds 0.5% [42].

3. Validation of Numerical Model

The results of the dynamic analysis were compared with the centrifuge test performed by Gillis [9] to validate the numerical model. Figure 3 shows the test layout, including the locations of the accelerometers and strain gauges. The bending moments in the centrifuge test were calculated from the strain sensor measurements. The centrifuge model was constructed at 1/65 scale, and the tests performed were at an acceleration of 65 g. Schofield [43] scaling laws were used to convert the measured responses from the centrifuge to the prototype scale. Medium dense dry Nevada sand ($D_{50} = 0.14$ mm, $C_u = 2.07$, $e_{\text{min}} = 0.53$, $e_{\text{max}} = 0.9$, and $G_s = 2.66$) was pluviated in the centrifuge container to achieve an initial relative density of $D_r \approx 55\%$. The unit weight of soil was 15.3 kN/m^3 . The shear wave velocity was measured from the bender element at two depths (8 m and 21.3 m) in the centrifuge. Owing to the limited recording available, the shear wave velocity profile was constructed using the following power law [44] such that it matches the available measurements at depths of 8 m and 21.3 m:

$$G_{\text{max}} = G_o \left(\frac{\sigma_m}{P_a} \right)^{0.5}, \quad (2)$$

where P_a is the atmospheric pressure and G_o is the curve fitting parameter ($G_o = 97348 \text{ kPa}$).

The properties of the tunnel structure and the estimated soil shear wave velocity for the centrifuge model are presented in Table 1 and Figure 4(a), respectively. The acceleration-time history and 5% damped acceleration response spectra of the input ground motion are shown in Figure 4(b). The characteristics of input motion are summarized in Table 2. Further details on the centrifuge are summarized in the study of Gillis [9]. The digitally measured data from the experiment were downloaded from the website <https://www.designsafe-ci.org> (last accessed on 09-01-2019) [45].

The numerical model to simulate the centrifuge test is shown in Figure 1, as explained in the previous section. As described in the previous section, 1D nonlinear analysis was performed to extract the EQL properties. The pressure-dependent nonlinear shear reduction curves proposed by Darendeli [46] were used. The over-consolidation ratio was set to 1.0, the horizontal at-rest earth pressure factor (K_0)

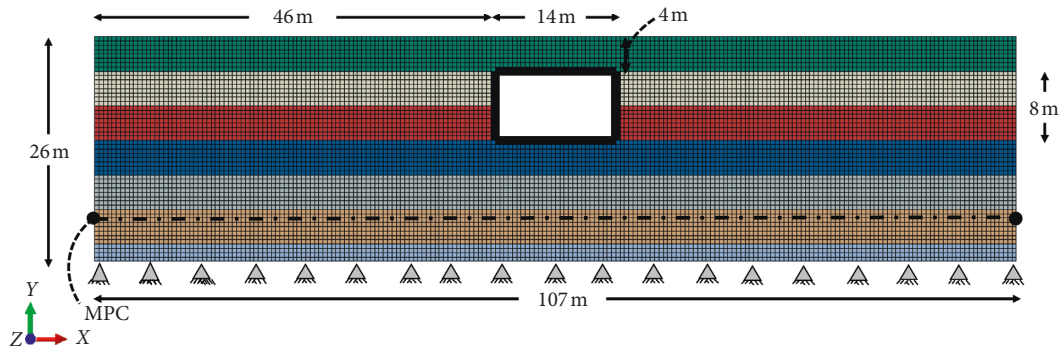


FIGURE 1: 2D FE model computational domain.

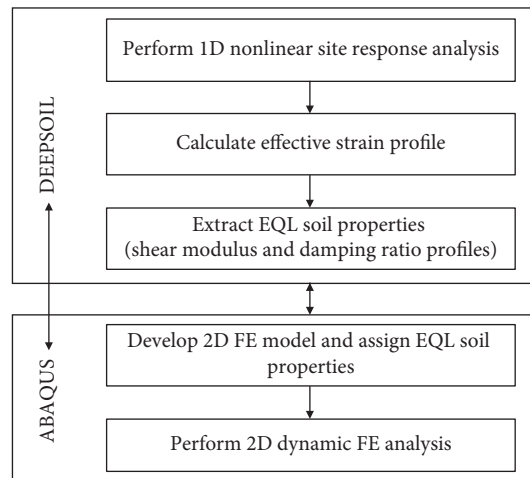


FIGURE 2: EQL history analysis procedure.

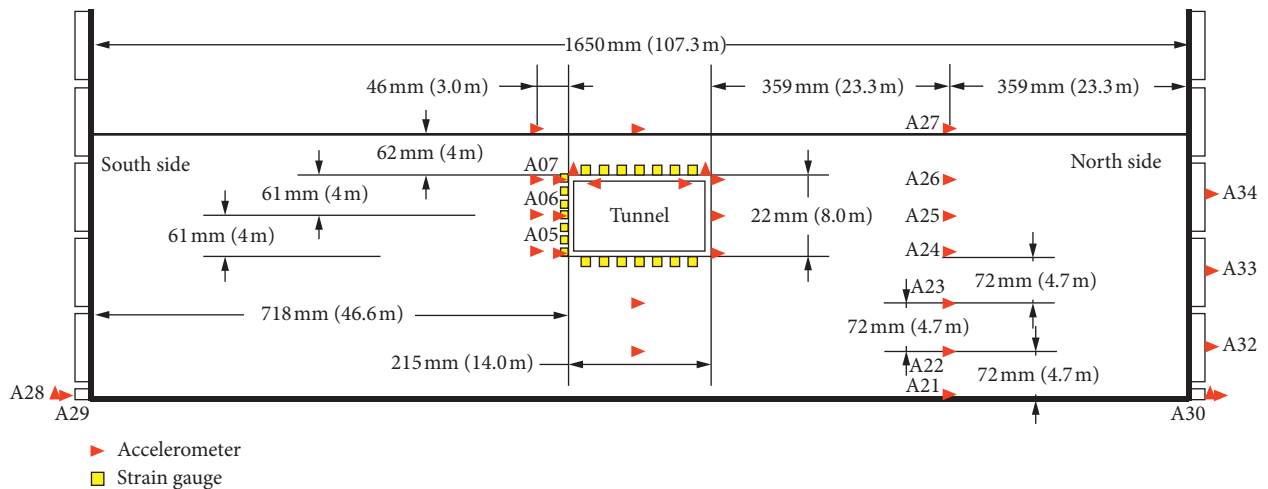


FIGURE 3: Centrifuge instrumentation layout indicating the accelerometers and strain gauge locations [9].

was set to 0.46, and the plasticity index (PI) was assumed as zero (0). The number of cycles of loading (N) and the excitation frequency (Hz) were defined as 10 and 1.0, respectively. Selected curves are illustrated in Figure 5. The maximum shear strain and the corresponding G/G_{max} and damping ratio profiles calculated from the 1D site response

analysis are shown in Figure 6. The extracted EQL properties are assigned to the FE model.

The computed responses from 2D FE analysis are shown in Figures 7–10. The calculated free-field peak ground acceleration (PGA) profiles and acceleration response spectra are compared with centrifuge measurements in

TABLE 1: Dimensions and properties of the tunnel in the centrifuge test [9].

Properties	
Size (m)	8 × 14
Thickness (m)	0.57
Material	6061 aluminium
Density (kg/m ³)	2700
Young's modulus (kPa)	6.89E + 07
Poisson's ratio	0.33
Racking stiffness (kN/m/m)	25,000 (2D frame analysis)

Figures 7(a) and 7(b), respectively. The free-field measurements, as shown in Figure 3, were made at a distance of 23.3 m from the right wall of the tunnel. The calculated responses were also extracted at the same distance from the tunnel. The measurements and calculations may have been influenced by the tunnel; in which case, the soil response cannot be strictly considered as free-field. Nonetheless, the soil responses are termed free-field in this paper to differentiate from the tunnel response. Comparisons demonstrate that the calculated free-field PGA profile and response spectra from EQL analysis match favourably with the measurements.

The measured and calculated peak accelerations at roof slab, midwall, and floor slab are compared in Figure 8(a). The response spectra at three locations in the tunnel are compared in Figure 8(b). Both the computed peak accelerations and the response spectra fit favourably with the centrifuge measurements, indicating that the numerical model is reliable. Comparison of calculated and measured increments of bending moment show that the fits are agreeable except at the top and bottom of the walls, as shown in Figure 9. It is because the wall-roof and wall-floor slab connections were modelled as rigid in the numerical model, whereas they were not perfectly rigid in the centrifuge model. Therefore, the numerical analysis produced higher bending moments.

The free-field and tunnel peak accelerations are compared in Figure 10(a). The ratio of the tunnel and free-field response spectra (RRS) is illustrated in Figure 10(b). It is shown that the tunnel produces higher accelerations compared with the free-field soil. The calculated value of F was 2.1 by using the following equation [31]:

$$F = \frac{G_m}{K} \frac{W}{H}, \quad (3)$$

where G_m is average strain-dependent shear modulus of the free-field ground along the height of the tunnel, K is the racking stiffness of the tunnel, and H and W are the height and width of the tunnel, respectively. K is defined as the reciprocal of lateral displacement caused by a unit concentrated force applied at the top of the tunnel and calculated from a frame analysis. In the frame model, the base is restrained against the translation degree of freedom and the joint rotation is allowed.

Because $F > 1$ indicates that the stiffness of the tunnel is lower than that of the surrounding soil, the tunnel response is larger relative to the free-field. The measurements highlight the importance of F on the seismic response of tunnels.

4. Parametric Study

The calibrated numerical model was used to investigate the effect of F on the tunnel response. The soil profile in the model was identical to that used in the centrifuge test. The EQL properties were again extracted from 1D nonlinear analyses performed using DEEPSOIL. The racking stiffness was calculated via a frame analysis. To investigate the effect of F , the axial (EA) and flexural rigidity of the tunnel were adjusted to achieve $F < 1$ (stiff tunnel) and $F > 1$ (flexible tunnel). The selected structural properties and racking stiffness for stiff and flexible tunnels are presented in Table 3. Two additional ground motions with long and short predominant periods were used, as shown in Table 4. The acceleration-time histories and response spectra are shown in Figure 11.

5. Results and Discussions

The raking deformation of the tunnel (Δ_{tunnel}) and the free-field displacement were extracted to compute R using the following equation:

$$R = \frac{\text{maximum}|\Delta_{\text{tunnel}}|}{\text{maximum}|\Delta_{\text{free-field}}|}, \quad (4)$$

where Δ_{tunnel} is calculated as the relative horizontal displacement between the tunnel top and bottom and $\Delta_{\text{free-field}}$ represents the relative free-field displacement at corresponding depths. The calculated values of F and R are compared with the F - R curve presented in NCHRP-611 [47] in Figure 12. The measured responses from the centrifuge test performed by Gillis [9] are also shown. The calculated F - R values fit very well with both NCHRP-611 [32] curve and Gillis [9] data points. It is shown that F has a pronounced influence on R , as observed in the centrifuge test. R is significantly lower for $F < 1$ tunnels than for $F > 1$ tunnels.

Figure 13 plots the ratio of acceleration response spectra (RRS) at the soil surface above the tunnel (location B) to the free-field surface (location A). For the stiff tunnel ($F < 1.0$), the calculated response above the tunnel is shown to be similar to the free-field soil. For the baseline and flexible tunnels, however, the spectral accelerations above the tunnels are 20–40% lower than the free-field soil at short periods up to 0.5 s. At longer periods up to 2.0 s, the stiff tunnel and baseline tunnel responses are similar to the free-field soil, whereas the flexible tunnel results in 10–20% amplification of the spectral acceleration. It is therefore highlighted that above-ground structures overlying underground structures should account for the influence of the underground structure on the propagated ground motion. However, the results presented here should only be used as a qualitative assessment and a site-specific evaluation should be performed to quantify the influence of the tunnel on the structure above it.

The dynamic thrust, which is calculated by integrating the seismically induced normal pressure along the tunnel wall at each time step, is an important parameter in the

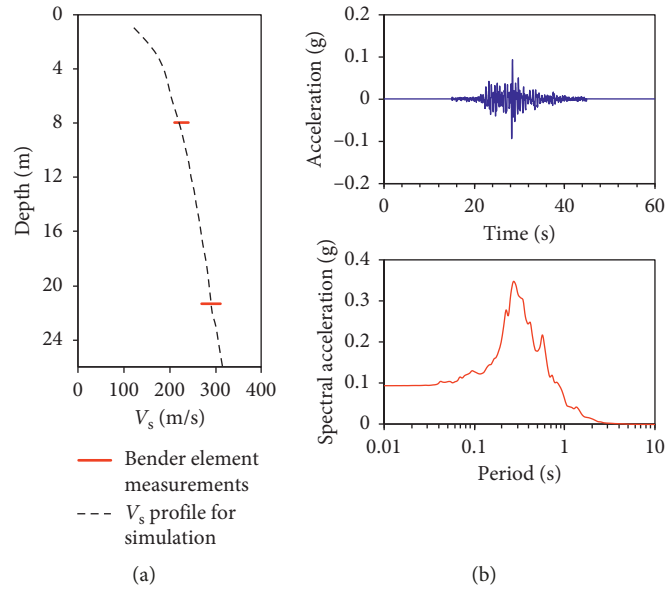


FIGURE 4: (a) Measured shear wave velocity profile [9]. (b) Input motion acceleration-time history and response spectra at the base of the centrifuge container.

TABLE 2: Characteristics of input motion [9].

Earthquake name	Year	Station name	PGA (g)	I_a (m/s)	D_{5-95} (s)	T_p (s)
Loma Prieta	1989	Santa Cruz	0.1	0.1	11.3	0.6

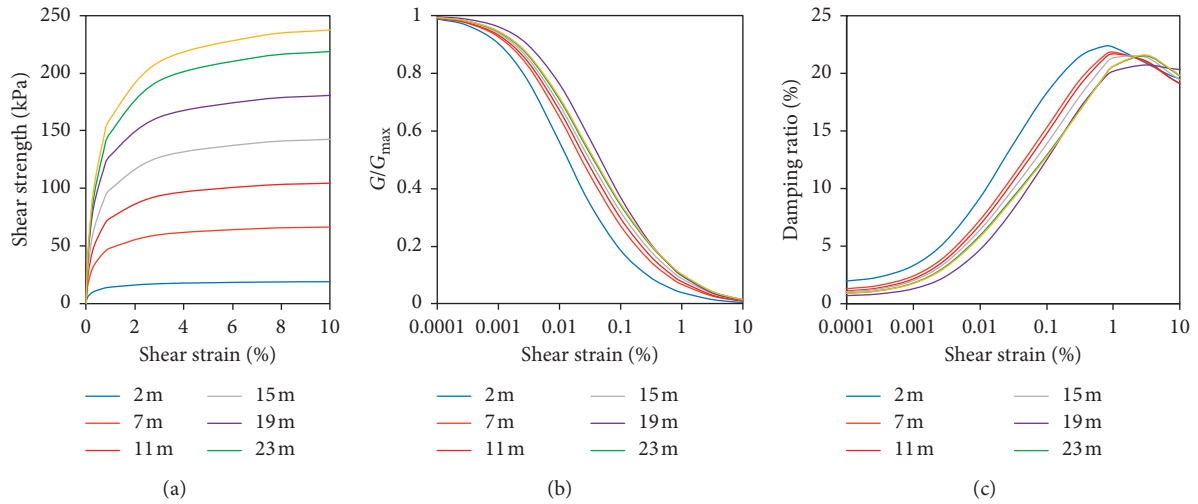


FIGURE 5: Calibrated nonlinear soil properties, (a) shear stress versus strain, (b) modulus reduction versus strains, and (c) damping versus strain curves [25].

seismic design of underground structures. In this the study, the maximum dynamic thrust is extracted and plotted against the free-field surface PGA in Figure 14. The effect of flexural rigidity on the dynamic thrust is considerable, showing 28% increase in the thrust for the flexible tunnel ($F > 1$) compared with the stiff tunnel ($F = 0.1$). The stiffer tunnel structure is shown to cause higher pressure even though R is lower. A nonlinear

increase in the dynamic increment of thrust with PGA is observed.

The calculated thrusts were also compared with the simplified analytical solutions for yielding walls, which were obtained via the Mononobe–Okabe method (Okabe [48]; Mononobe [49]) and the Seed and Whitman [50] procedure. It is demonstrated that Mononobe–Okabe and Seed and Whitman [50] methods developed for yielding walls are too

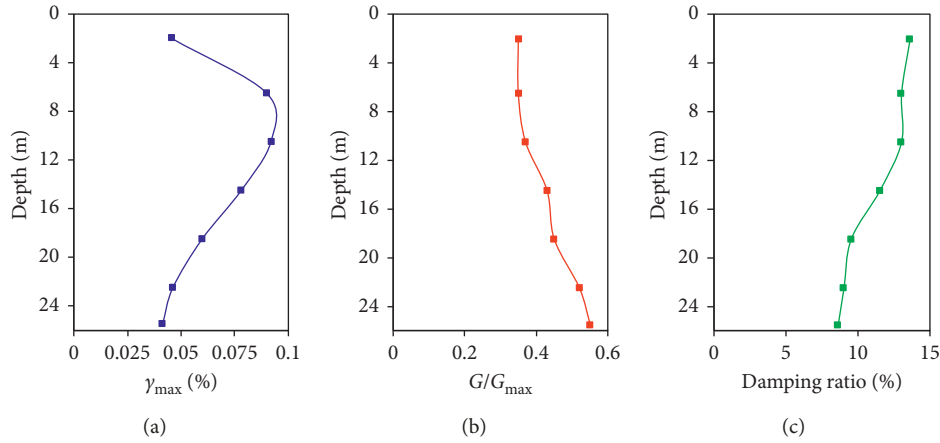


FIGURE 6: The results calculated from 1D nonlinear site response analysis: (a) maximum shear strain profile, (b) G/G_{max} profile, and (c) damping ratio profile.

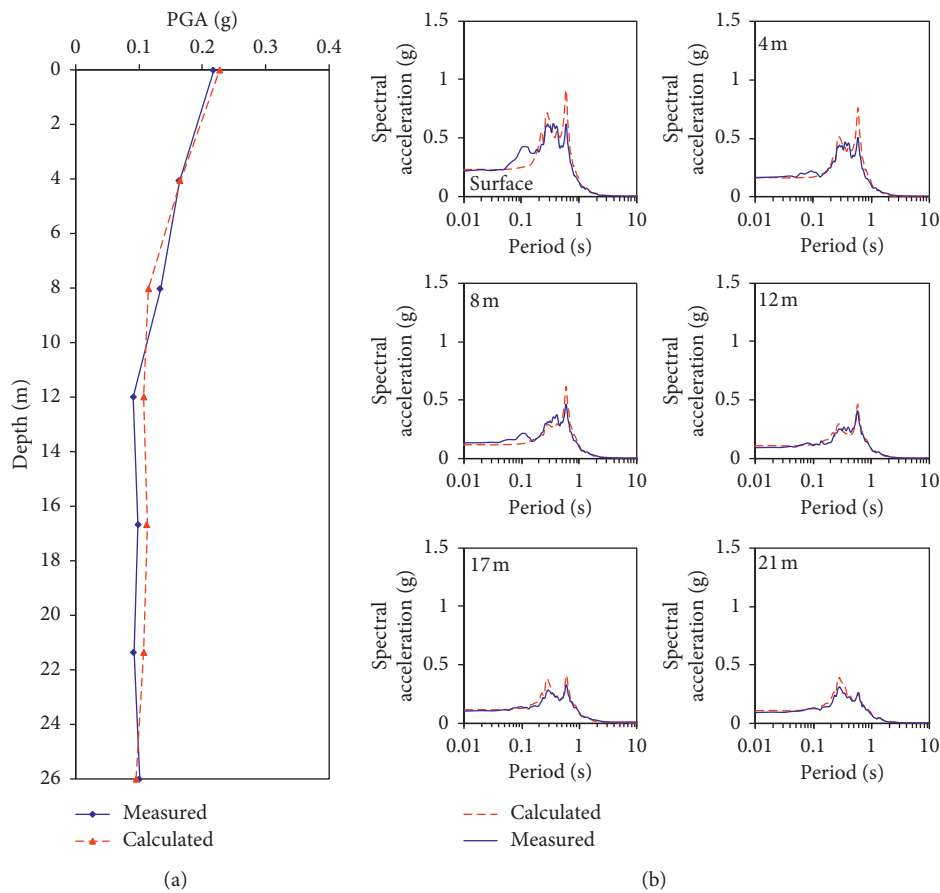


FIGURE 7: Comparison of the measured and calculated free-field responses. (a) PGA profile. (b) Acceleration response spectra at various depths.

conservative. This is because (1) the earth pressure equation for yielding walls does not account for F and (2) the reduction in the peak acceleration with depth is not simulated. A comparison with the equation of Wood [51] widely used for embedded box structures is not presented because this equation will result in even higher thrust. Based on the foregoing results, it is highlighted that the earth pressure

developed for yielding walls or a rigid box are too conservative to be used in the seismic design of underground tunnels.

Figure 15 plots the time histories of acceleration and shear strain calculated at the middepth of the tunnel along with the dynamic thrust for the stiff tunnel. The timing of the maximum dynamic thrust is shown to be close to those of

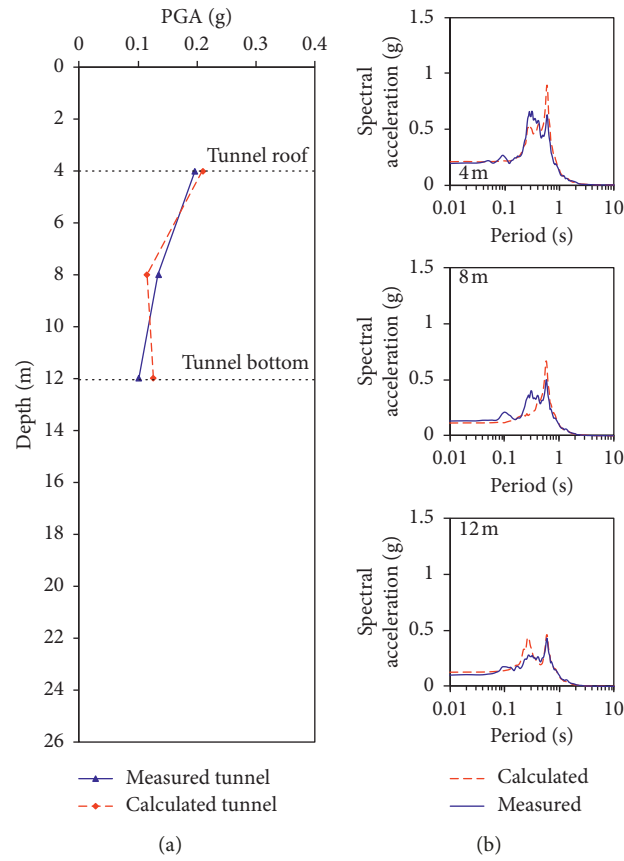


FIGURE 8: Comparison of the measured and calculated tunnel responses. (a) PGA profile. (b) Acceleration response spectra at top slab (4 m), midwall (8 m), and bottom floor (12 m) of the tunnel.

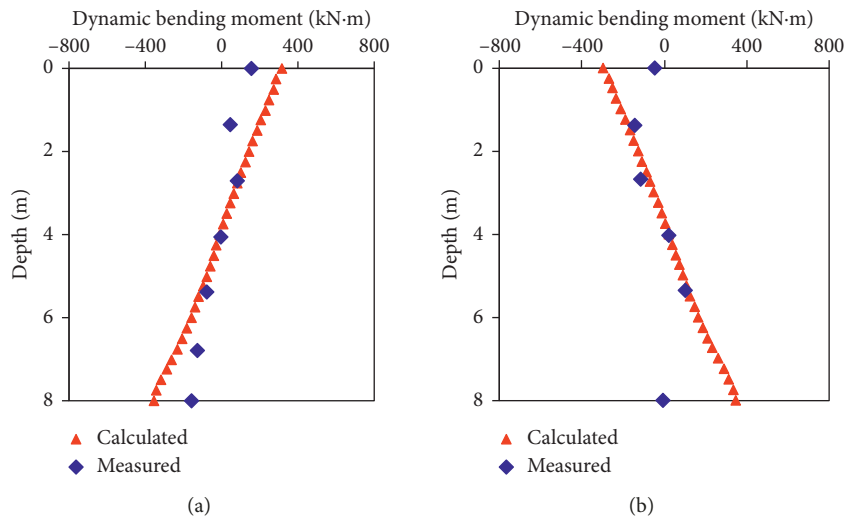


FIGURE 9: Continued.

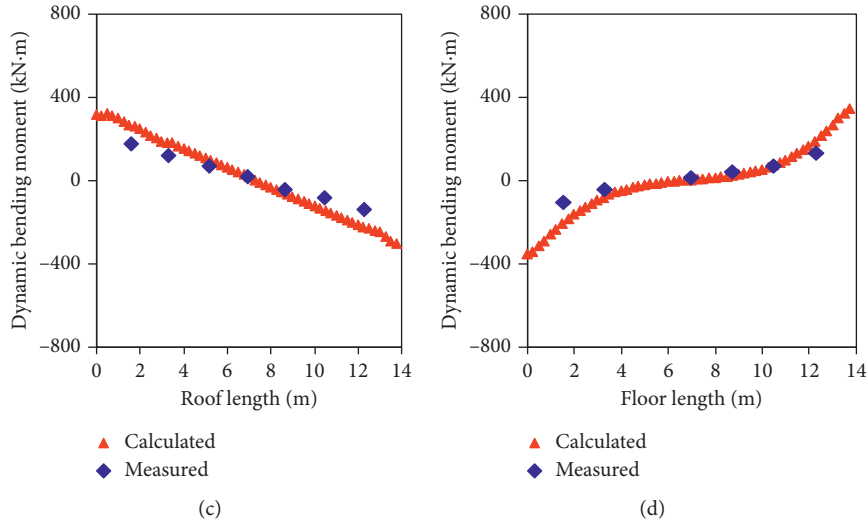


FIGURE 9: Comparison of measured and calculated dynamic bending moments at maximum thrust. (a) North-side tunnel wall. (b) South-side tunnel wall. (c) Roof slab. (d) Floor slab.

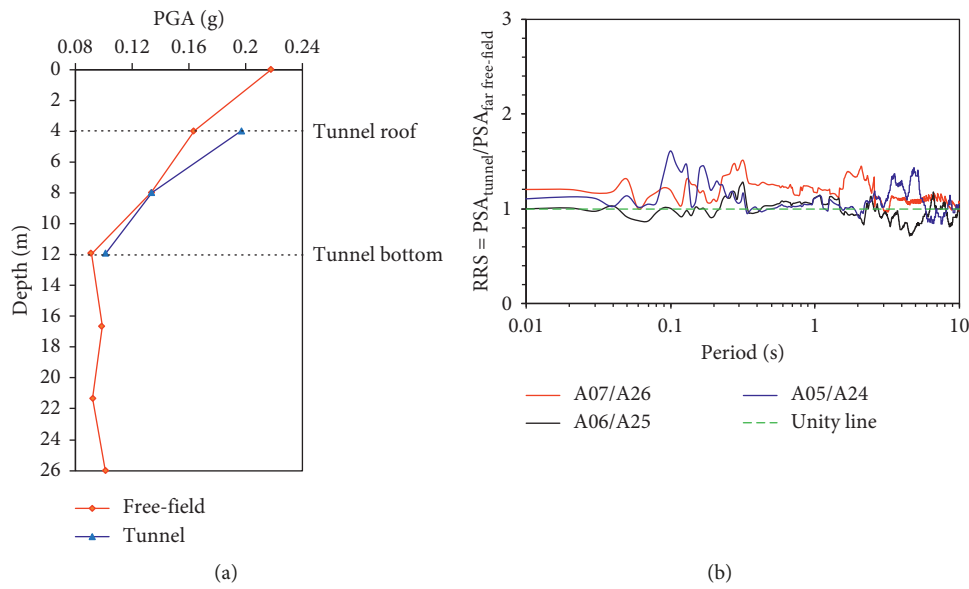


FIGURE 10: Evidence of the influence of F on tunnel response from the centrifuge test. (a) PGA profiles at free-field and tunnel wall. (b) RRS of the tunnel and free-field responses (A07 = tunnel roof; A06 = tunnel spring line, A05 = tunnel floor; A26, A25, A24 = free-field responses at corresponding depths).

TABLE 3: Study matrix representing the properties of tunnel structure used in this study.

Structure	Thickness (m)	Young's modulus (kPa)	Racking stiffness (kN/m/m)	Remarks
Stiff	1.5	$3.93E+07$	233,395	Centrifuge
Baseline	0.8	$2.5E+07$	25,842	
Flexible	0.4	$2.35E+07$	3,263	

TABLE 4: Characteristics of earthquake ground motion used in the study.

Earthquake name	Year	Station name	PGA (g)	I_a (m/s)	D_{5-95} (s)	T_P (s)
Nahanni	1985	Site 3	0.17	0.2	6	0.06
Chi-Chi	1999	CHY-047	0.18	1.1	34.9	0.54

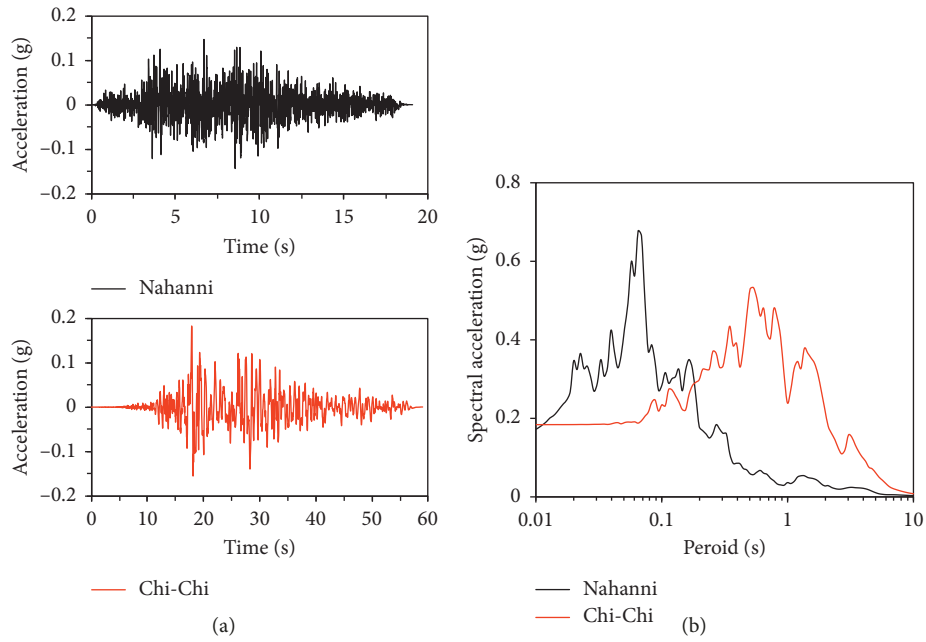


FIGURE 11: Additional earthquake ground motions. (a) Acceleration-time histories. (b) Acceleration response spectra.

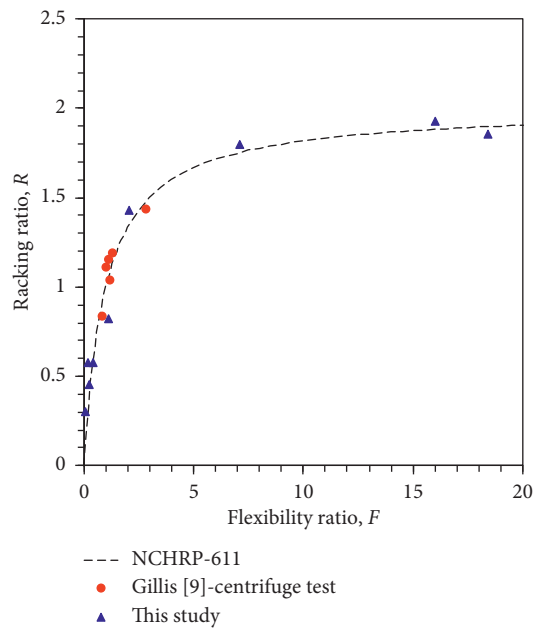


FIGURE 12: Comparison of racking and flexibility ratio (F - R) relationship NCHRP-611 report [32] and centrifuge tests of Gillis [9].

PGA and maximum shear strain, except for the Nahanni motion. It was reported that the underground structure response is highly dependent on the ground deformation, and therefore, the peak ground velocity (PGV) or shear strain is an ideal index to estimate the performance of tunnels [52]. Figure 16 plots the ratio of the bending moment, thrust, and shear stress extracted at maximum dynamic thrust to the calculated response determined at maximum shear strain. Except for the bending moment, the ratios are very close to unity. It is therefore demonstrated

that the response can be either extracted at the time step of maximum thrust or shear strain. In the following section, the responses were extracted at the timing of the maximum dynamic thrust, as has widely been used in previous studies [9, 53, 54].

Figure 17 shows a comparison of the maximum absolute surface soil settlement envelope. Figure 18 shows the deformed tunnel shape (magnified 50 times) plotted at the time step of maximum dynamic thrust. F is shown to influence both the surface settlement distribution and

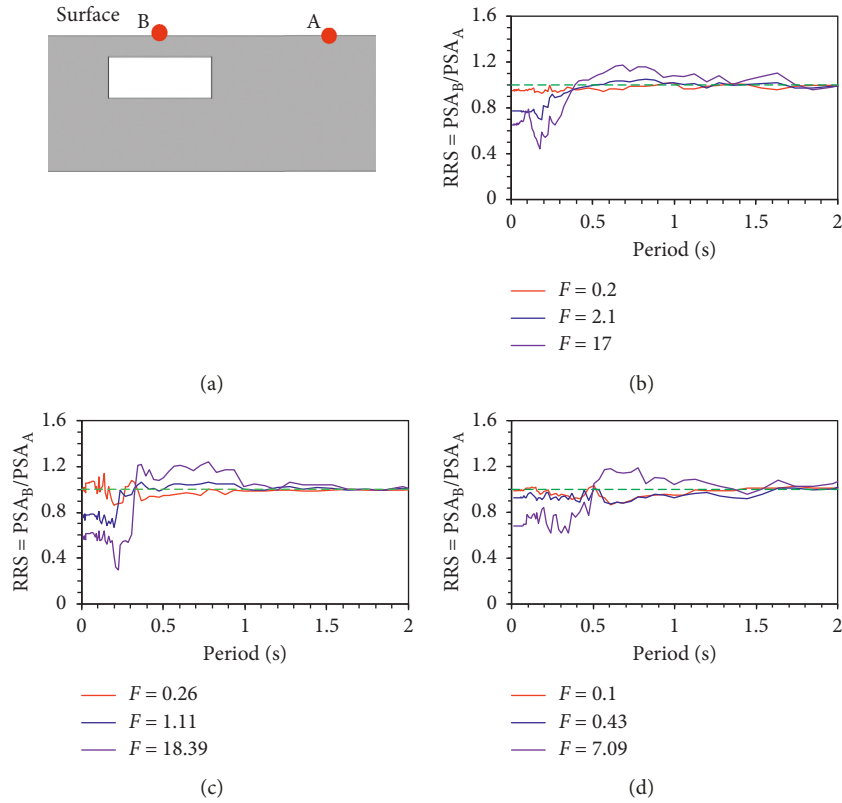


FIGURE 13: Surface RRS (a) comparison for various F ratios for (b) Loma Prieta, (c) Nahanni, and (d) Chi-Chi motions.

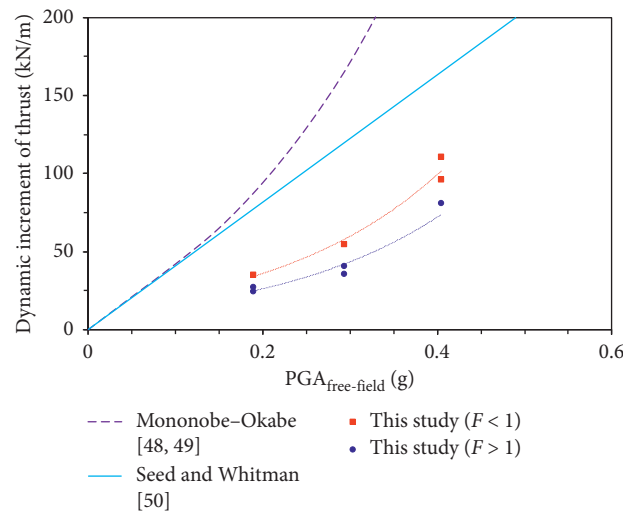


FIGURE 14: Comparison of computed dynamic increment of thrust with available analytical solution.

the peak settlement. It is interesting that slight heaving patterns at the surface are observed in rigid tunnels ($F < 1$), whereas flexible tunnels ($F > 1$) exhibited settlement at the center of the roof slab. The surface settlement was closely related to the tunnel deformation shape. For stiff tunnels, convex deformation in the floor slab was observed, whereas the roof slab shape was not greatly altered. This is likely to have caused the tunnel to move

upward, resulting in heaving at the surface. For flexible tunnels ($F > 1$), both the floor and roof slabs underwent convex bending, causing heaving at the floor and settlement at the roof. For highly flexible tunnels, the settlement can exceed 40 mm. It should be noted that the calculated settlement is likely to be influenced by the constitutive model. Although the EQL approach has been shown to provide reliable estimates of the shear

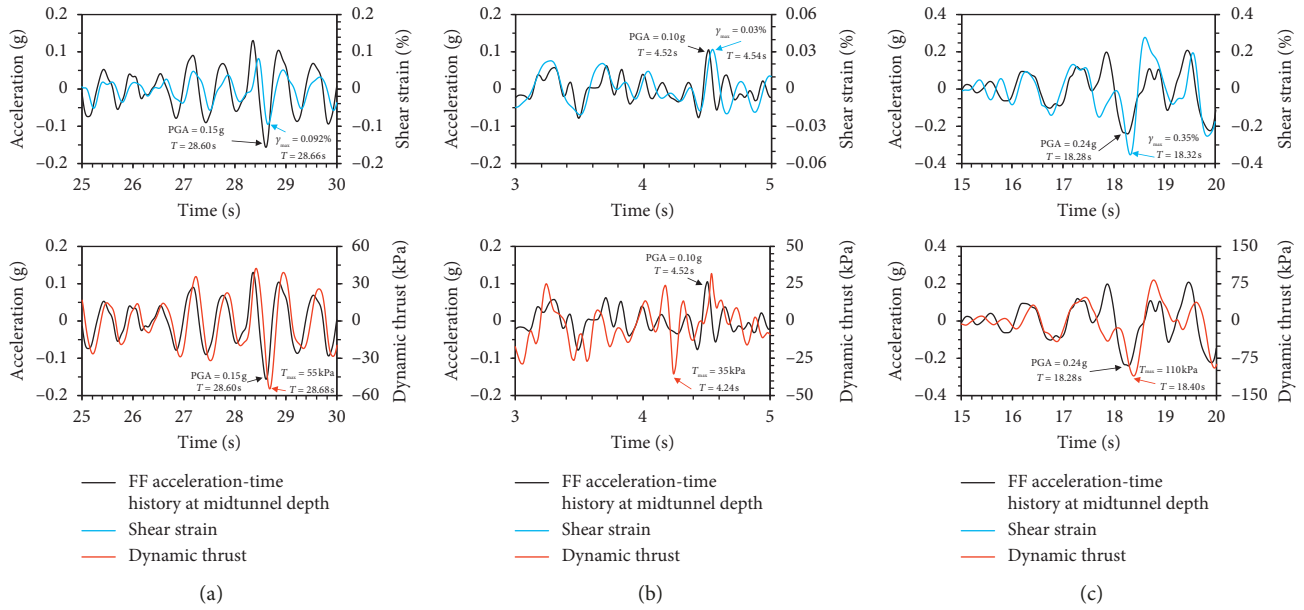


FIGURE 15: Comparison of free-field acceleration at tunnel middepth, shear strain, and dynamic increment of thrust in stiff soil-tunnel configuration for (a) Loma Prieta, (b) Nahanni, and (c) Chi-Chi motions.

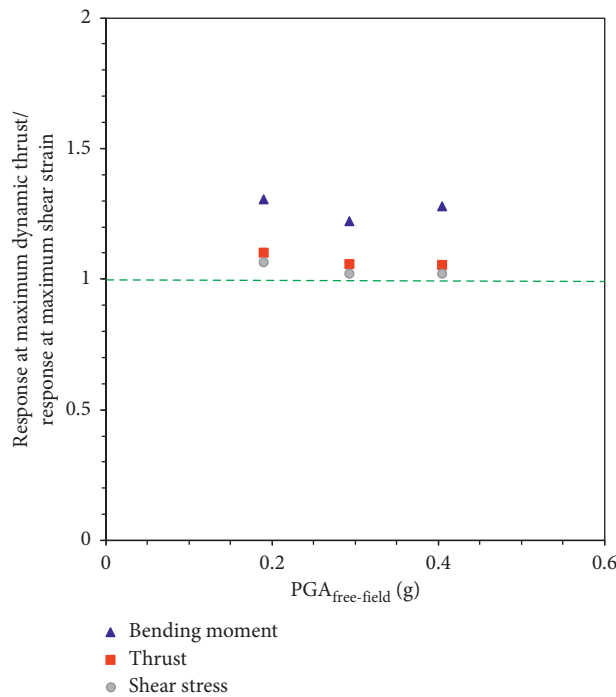


FIGURE 16: Ratio of extracted maximum responses of tunnel at time step of maximum thrust and maximum shear strain.

deformation, the accuracy of the settlement prediction has not yet been validated. Further studies are warranted to investigate the sensitivity of the constitutive model on the predicted settlement and whether the EQL analysis can be used to estimate the settlement. Therefore, the surface deformation calculations should only be used as a qualitative evaluation.

The peak shear stress around the tunnel lining is shown in Figure 19. As expected, flexible tunnels induced higher stress than the stiff tunnels. The maximum shear stresses developed at the corners of the tunnel perimeter. Sharp increments in the shear stresses were observed for the flexible tunnel subjected to Loma Prieta and Nahanni motions.

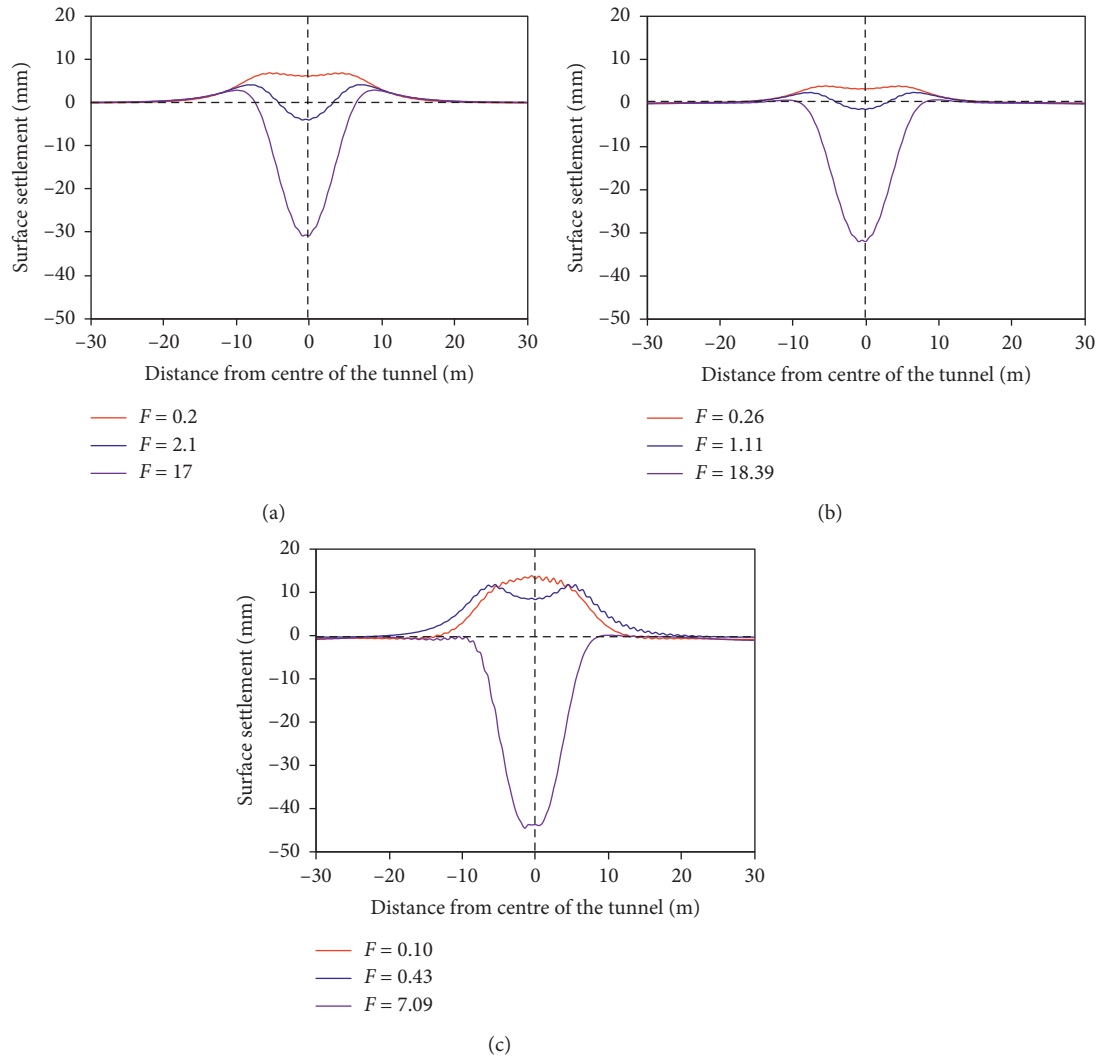


FIGURE 17: Surface settlement envelope for (a) Loma Prieta, (b) Nahanni, and (c) Chi-Chi motions.



(a)

FIGURE 18: Continued.

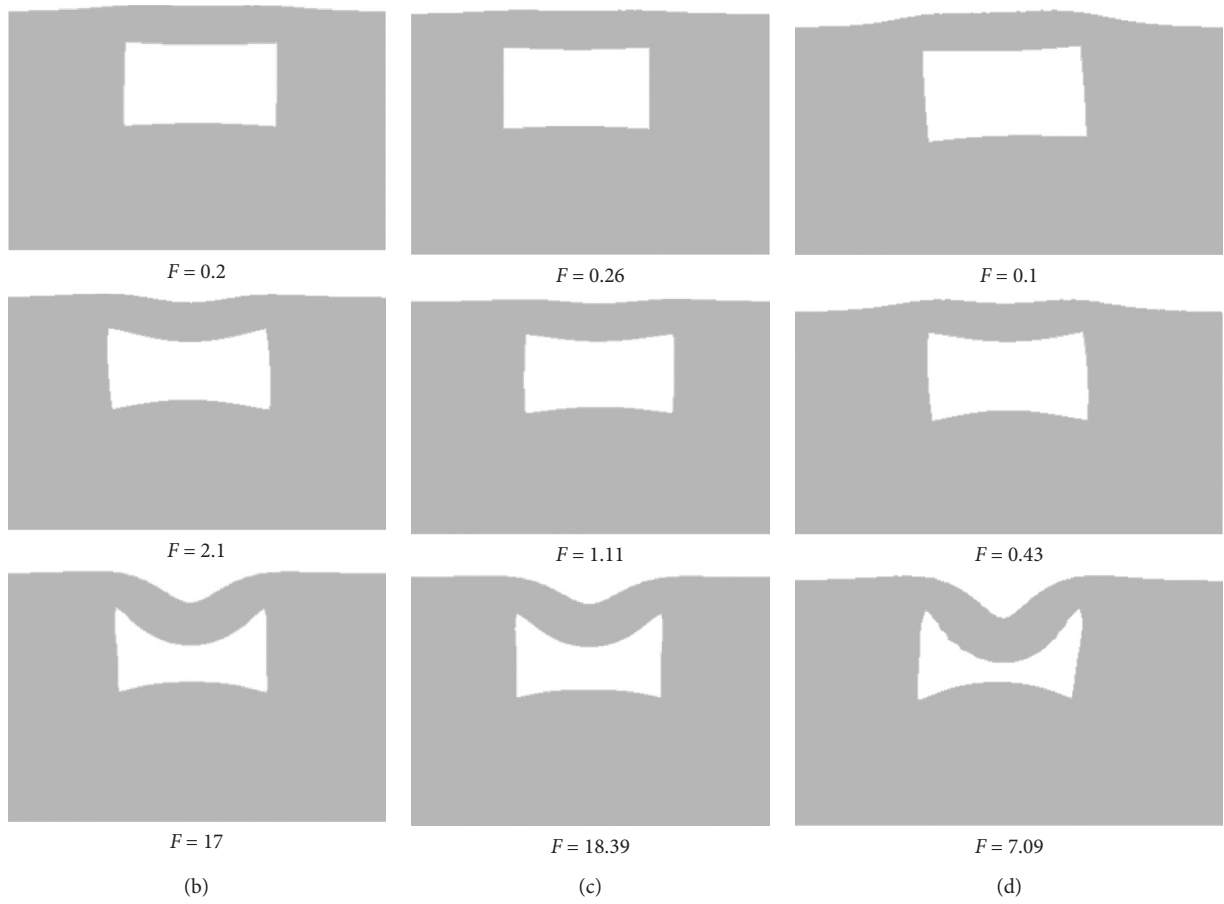
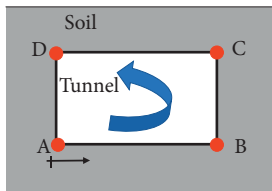
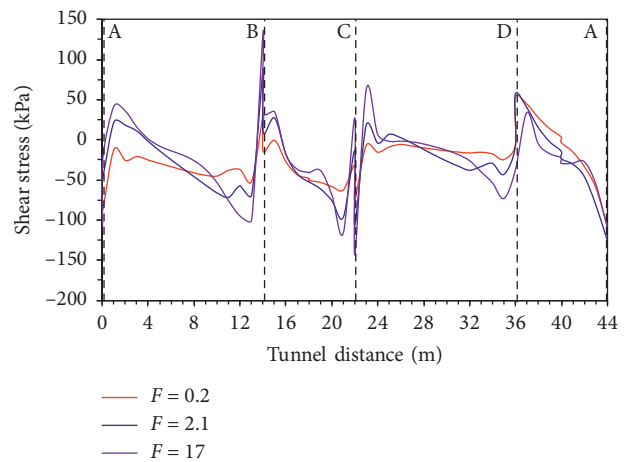


FIGURE 18: (a) Undeformed shape. Deformed shapes (scale factor = 50 magnification) plotted at time step of maximum thrust for (b) Loma Prieta, (c) Nahanni, and (d) Chi-Chi motions.



(a)



(b)

FIGURE 19: Continued.

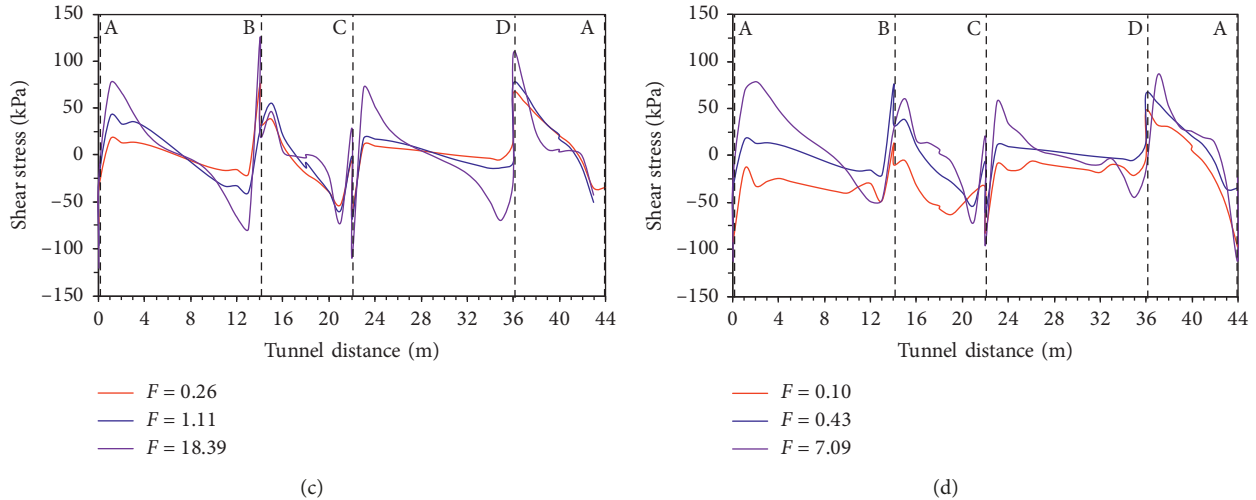


FIGURE 19: Shear stress distribution (a) at soil elements adjacent to tunnel at time of maximum thrust for (b) Loma Prieta, (c) Nahanni, and (d) Chi-Chi motions.

6. Conclusions

A series of EQL dynamic analyses were performed to evaluate the seismic response of cut-and-cover rectangular tunnels. The numerical model was validated against the measurements from the centrifuge experiment. The comparisons showed that both the measured free-field and tunnel acceleration response spectra fit favourably with numerical simulation. A series of numerical analyses were performed to investigate the influence of F on the tunnel response. The conclusions derived from this study are the following:

- (1) F of the tunnel has pronounced influence on its acceleration.
- (2) F of the tunnel is positively correlated to R . The available NCHRP-611 F - R curve is demonstrated to be reliable for estimating tunnel deformation when average free-field effective strain-compatible shear modulus (G_m) computed from 1D site response analysis is used to calculate F .
- (3) None of the simplified earth pressure solutions for yielding walls or embedded box structure was shown to provide reliable estimate of the dynamic increment of thrust regardless of peak acceleration level and F . It is therefore recommended not to use the earth pressure equation in the design of underground tunnels.
- (4) F of the tunnel significantly influences the tunnel deformation pattern as well as surface settlement distribution. Stiff tunnels may experience heaving at the surface because of the convex bending of the floor slab, whereas the roof slab undergoes limited deformation. Flexible tunnels are shown to produce convex bending in both the floor and roof slabs. A significant level of surface settlement may occur at the surface for highly flexible box tunnels.

- (5) Increase in F causes a corresponding increase in the shear stress around the tunnel lining. Additionally, sharp peaks of shear stress can also develop at the corners for flexible tunnels.

Notations

F :	Flexibility ratio
R :	Racking ratio
EQL:	Equivalent linear
NCHRP:	National Cooperative Highway Research Program
2D:	Two dimensional
CPE4R:	Four-node plane strain element with reduced integration
B21:	Two-node beam element
MPCs:	Multipoint constraints
φ_{soil} :	Friction angle of soil
1D:	One dimensional
K_0 :	Horizontal at-rest earth pressure factor
PI:	Plasticity index
f :	Excitation frequency
HZ:	Hertz
MRDF:	Modulus reduction and damping curve fitting procedure
I_a :	Arias intensity
D_{5-95} :	Significant duration
T_p :	Predominant period
G/G_{max} :	Normalized shear modulus
D_{50} :	Particle diameter at 50% in the cumulative distribution
C_u :	Uniformity coefficient
e_{min} :	Minimum void ratio
e_{max} :	Maximum void ratio
G_s :	Specific gravity of soil
D_r :	Relative density of soil
G_o :	Reference shear modulus of soil
G_{max} :	Small strain shear modulus of soil
P_a :	Atmospheric pressure

σ_m :	Mean confining stress
V_s :	Soil shear wave velocity
Δl :	Numerical mesh size
λ :	Wavelength of input ground motion
Δ_{tunnel} :	Tunnel racking displacement
$\Delta_{\text{free-field}}$:	Free-field racking displacement
PGA:	Peak ground acceleration
RRS:	Ratio of response spectra
G_m :	Strain-dependent shear modulus
K :	Racking stiffness of the tunnel
H :	Height of the tunnel
W :	Width of the tunnel
γ_{max} :	Maximum free-field shear strain.

Data Availability

The measured data of Gillis [9] centrifuge was used to validate the numerical model and can be downloaded from the Design Safe website <https://www.designsafe-ci.org> (last accessed on 09-01-2019) [45]. The digital data of input ground motions used for parametric study can also be downloaded from NGA-WEST2 website <https://ngawest2.berkeley.edu> (last accessed on 09-01-2019).

Conflicts of Interest

The authors declare no conflicts of interest.

Acknowledgments

This research was supported by a grant (18SCIP-B146946-01) from the Construction Technology Research Program funded by Ministry of Land, Infrastructure and Transport of Korean Government.

References

- [1] N. Yoshida and S. Nakamura, "Damage to Daikai subway station during the 1995 Hyogoken-Nunbu earthquake and its investigation," in *Proceedings of the Eleventh World Conference on Earthquake Engineering*, pp. 283–300, Acapulco, Mexico, June 1996.
- [2] J. C. Chou, B. L. Kutter, T. Travararou, and J. M. Chacko, "Centrifuge modeling of seismically induced uplift for the BART transbay tube," *Journal of Geotechnical and Geoenvironmental Engineering*, vol. 137, no. 8, pp. 754–765, 2011.
- [3] S. Shibayama, J. Izawa, A. Takahashi, J. Takemura, and O. Kusakabe, "Observed behaviour of a tunnel in sand subjected to shear deformation in a centrifuge," *Soils and Foundations*, vol. 50, no. 2, pp. 281–294, 2010.
- [4] U. Cilingir and S. P. G. Madabhushi, "Effect of depth on the seismic response of square tunnels," *Soils and Foundations*, vol. 51, no. 3, pp. 449–457, 2011.
- [5] G. Tsinidis, K. Pitilakis, G. Madabhushi, and C. Heron, "Dynamic response of flexible square tunnels: centrifuge testing and validation of existing design methodologies," *Géotechnique*, vol. 65, no. 5, pp. 401–417, 2015.
- [6] G. Tsinidis, K. Pitilakis, and G. Madabhushi, "On the dynamic response of square tunnels in sand," *Engineering Structures*, vol. 125, pp. 419–437, 2016.
- [7] G. Tsinidis, "Response characteristics of rectangular tunnels in soft soil subjected to transversal ground shaking," *Tunnelling and Underground Space Technology*, vol. 62, pp. 1–22, 2017.
- [8] A. Hushmand, S. Dashti, C. Davis, J. S. McCartney, and B. Hushmand, "A centrifuge study of the influence of site response, relative stiffness, and kinematic constraints on the seismic performance of buried reservoir structures," *Soil Dynamics and Earthquake Engineering*, vol. 88, pp. 427–438, 2016.
- [9] K. M. Gillis, "Seismic response of shallow underground structures in dense urban environments," Ph.D. dissertation, Dept. of Civil, Environmental and Architectural Engineering, University of Colorado at Boulder, Boulder, CO, USA, 2015.
- [10] E. Bilotta, G. Lanzano, S. P. G. Madabhushi, and F. Silvestri, "A numerical round robin on tunnels under seismic actions," *Acta Geotechnica*, vol. 9, no. 4, pp. 563–579, 2014.
- [11] G. Abate, M. R. Massimino, and M. Maugeri, "Numerical modelling of centrifuge tests on tunnel-soil systems," *Bulletin of Earthquake Engineering*, vol. 13, no. 7, pp. 1927–1951, 2015.
- [12] H. Xu, T. Li, L. Xia, J. X. Zhao, and D. Wang, "Shaking table tests on seismic measures of a model mountain tunnel," *Tunnelling and Underground Space Technology*, vol. 60, pp. 197–209, 2016.
- [13] I. Shahrour, F. Khoshnoudian, M. Sadek, and H. Mroueh, "Elastoplastic analysis of the seismic response of tunnels in soft soils," *Tunnelling and Underground Space Technology*, vol. 25, no. 4, pp. 478–482, 2010.
- [14] G. Wang, M. Yuan, Y. Miao, J. Wu, and Y. Wang, "Experimental study on seismic response of underground tunnel-soil-surface structure interaction system," *Tunnelling and Underground Space Technology*, vol. 76, pp. 145–159, 2018.
- [15] X. Yan, J. Yuan, H. Yu, A. Bobet, and Y. Yuan, "Multi-point shaking table test design for long tunnels under non-uniform seismic loading," *Tunnelling and Underground Space Technology*, vol. 59, pp. 114–126, 2016.
- [16] M. R. Moghadam and M. H. Baziar, "Seismic ground motion amplification pattern induced by a subway tunnel: shaking table testing and numerical simulation," *Soil Dynamics and Earthquake Engineering*, vol. 83, pp. 81–97, 2016.
- [17] Z.-Y. Chen, W. Chen, and W. Zhang, "Seismic performance evaluation of multi-story subway structure based on pushover analysis," in *Proceedings of the Advances in Soil Dynamics and Foundation Engineering*, pp. 444–454, Shanghai, China, May 2014.
- [18] C. Guoxing, C. Su, Z. Xi, D. Xiuli, Q. Chengzhi, and W. Zhihua, "Shaking-table tests and numerical simulations on a subway structure in soft soil," *Soil Dynamics and Earthquake Engineering*, vol. 76, pp. 13–28, 2015.
- [19] Z. Bao, Y. Yuan, and H. Yu, "Multi-scale physical model of shield tunnels applied in shaking table test," *Soil Dynamics and Earthquake Engineering*, vol. 100, pp. 465–479, 2017.
- [20] H. Huo, A. Bobet, G. Fernández, and J. Ramírez, "Load transfer mechanisms between underground structure and surrounding ground: evaluation of the failure of the Daikai station," *Journal of Geotechnical and Geoenvironmental Engineering*, vol. 131, no. 12, pp. 1522–1533, 2005.
- [21] I. Anastasopoulos, N. Gerolymos, V. Drosos, R. Kourkoulis, T. Georgarakos, and G. Gazetas, "Nonlinear response of deep immersed tunnel to strong seismic shaking," *Journal of Geotechnical and Geoenvironmental Engineering*, vol. 133, no. 9, pp. 1067–1090, 2007.
- [22] S. Kontoe, L. Zdravkovic, D. M. Potts, and C. O. Menkiti, "On the relative merits of simple and advanced constitutive models in dynamic analysis of tunnels," *Géotechnique*, vol. 61, no. 10, pp. 815–829, 2011.

- [23] M. H. Baziar, M. R. Moghadam, D.-S. Kim, and Y. W. Choo, "Effect of underground tunnel on the ground surface acceleration," *Tunnelling and Underground Space Technology*, vol. 44, pp. 10–22, 2014.
- [24] M. H. Baziar, M. R. Moghadam, Y. W. Choo, and D.-S. Kim, "Tunnel flexibility effect on the ground surface acceleration response," *Earthquake Engineering and Engineering Vibration*, vol. 15, no. 3, pp. 457–476, 2016.
- [25] Y. M. A. Hashash, S. Dashti, M. Musgrove et al., "Influence of tall buildings on seismic response of shallow underground structures," *Journal of Geotechnical and Geoenvironmental Engineering*, vol. 144, no. 12, article 04018097, 2018.
- [26] T.-H. Lee, D. Park, D. D. Nguyen, and J.-S. Park, "Damage analysis of cut-and-cover tunnel structures under seismic loading," *Bulletin of Earthquake Engineering*, vol. 14, no. 2, pp. 413–431, 2016.
- [27] K. Pitilakis and G. Tsinidis, "Performance and seismic design of underground structures," in *Earthquake Geotechnical Engineering Design*, M. Maugeri and C. Soccodato, Eds., pp. 279–340, Springer International Publishing, Cham, Switzerland, 2014.
- [28] G. Abate, S. Corsico, and M. R. Massimino, "FEM modelling of the seismic behavior of a tunnel-soil-aboveground building system: a case history in Catania (Italy)," *Procedia Engineering*, vol. 158, pp. 380–385, 2016.
- [29] G. Abate and M. R. Massimino, "Parametric analysis of the seismic response of coupled tunnel-soil-aboveground building systems by numerical modelling," *Bulletin of Earthquake Engineering*, vol. 15, no. 1, pp. 443–467, 2017.
- [30] Y. X. Wang, S. B. Shan, C. Zhang, and P. P. Guo, "Seismic response of tunnel lining structure in a thick expansive soil stratum," *Tunnelling and Underground Space Technology*, vol. 88, pp. 250–259, 2019.
- [31] J.-N. Wang, *Seismic Design of Tunnels: A Simple State-of-the-Art Design Approach*, Parsons Brinckerhoff, New York, NY, USA, 1993.
- [32] D. G. Anderson, G. R. Martin, I. P. Lam, and J. N. Wang, *Seismic Analysis and Design of Retaining Walls, Buried Structures, Slopes, and Embankments*, Transportation Research Board, Washington, DC, USA, 2008.
- [33] ABAQUS, *Analysis User's Manual, Version 6.12*, Dassault Systèmes Simulia Corporation, Johnston, RI, USA, 2012.
- [34] Y. H. Deng, S. Dashti, A. Hushmand, C. Davis, and B. Hushmand, "Seismic response of underground reservoir structures in sand: evaluation of class-C and C1 numerical simulations using centrifuge experiments," *Soil Dynamics and Earthquake Engineering*, vol. 85, pp. 202–216, 2016.
- [35] W. Zhang, E. E. Seylabi, and E. Taciroglu, "Validation of a three-dimensional constitutive model for nonlinear site response and soil-structure interaction analyses using centrifuge test data," *International Journal for Numerical and Analytical Methods in Geomechanics*, vol. 41, no. 18, pp. 1828–1847, 2017.
- [36] R. L. Kuhlemeyer and J. Lysmer, "Finite element method accuracy for wave propagation problems," *Journal of Soil Mechanics & Foundations Division*, vol. 99, no. 5, pp. 421–427, 1973.
- [37] S. Argyroudis, G. Tsinidis, F. Gatti, and K. Pitilakis, "Effects of SSI and lining corrosion on the seismic vulnerability of shallow circular tunnels," *Soil Dynamics and Earthquake Engineering*, vol. 98, pp. 244–256, 2017.
- [38] Y. M. A. Hashash, M. I. Musgrove, J. A. Harmon et al., *DEEPSOIL 7.0, User Manual*, University of Illinois at Urbana-Champaign, Champaign, IL, USA, 2017.
- [39] C. Phillips and Y. M. A. Hashash, "Damping formulation for nonlinear 1D site response analyses," *Soil Dynamics and Earthquake Engineering*, vol. 29, no. 7, pp. 1143–1158, 2009.
- [40] D. R. Groholski, Y. M. A. Hashash, M. T. Musgrove, J. E. Harmon, and B. S.-H. Kim, "Evaluation of 1-D non-linear site response analysis using a general quadratic/hyperbolic strength-controlled constitutive model," in *Proceedings of the 6th International Conference on Earthquake Geotechnical Engineering*, pp. 1–4, Christchurch, New Zealand, November 2015.
- [41] A. O. L. Kwok, J. P. Stewart, Y. M. A. Hashash et al., "Use of exact solutions of wave propagation problems to guide implementation of nonlinear seismic ground response analysis procedures," *Journal of Geotechnical and Geoenvironmental Engineering*, vol. 133, no. 11, pp. 1385–1398, 2007.
- [42] B. Kim, Y. M. A. Hashash, J. P. Stewart et al., "Relative differences between nonlinear and equivalent-linear 1-D site response analyses," *Earthquake Spectra*, vol. 32, no. 3, pp. 1845–1865, 2016.
- [43] A. N. Schofield, "Dynamic and earthquake geotechnical centrifuge modelling," in *Proceedings of the International Conference on Recent Advances in Geotechnical Earthquake Engineering and Soil Dynamics*, University of Missouri, Rolla, MO, USA, April 1981.
- [44] F. E. Richart Jr., "Some effects of dynamic soil properties on soil-structure interaction," *Journal of Geotechnical Geoenvironmental Engineering*, vol. 101, no. 12, pp. 1193–1240, 1975.
- [45] E. M. Rathje, C. Dawson, J. E. Padgett et al., "DesignSafe: new cyberinfrastructure for natural hazards engineering," *Natural Hazards Review*, vol. 18, no. 3, article 06017001, 2017.
- [46] M. B. Darendeli, "Development of a new family of normalized modulus reduction and material damping curves," Ph.D. dissertation, University of Texas at Austin, Austin, TX, USA, 2001.
- [47] D. G. Anderson, *Seismic Analysis and Design of Retaining Walls, Buried Structures, Slopes, and Embankments*, Transportation Research Board, Washington, DC, USA, 2008.
- [48] N. Okabe, "General theory on earth pressure and seismic stability of retaining wall and dam," *Journal of Japan Society of Civil Engineering*, vol. 10, no. 6, pp. 1277–1323, 1924.
- [49] N. Mononobe, "On determination of earth pressure during earthquake," in *Proceedings of the World Engineering Congress*, pp. 177–185, Tokyo, Japan, 1929.
- [50] H. B. Seed and R. V. Whitman, "Design of earth retaining structures for dynamic loads," in *Proceedings of the ASCE Specialty Conference-Lateral Stress in the Ground and Design of Earth Retaining Structures*, Ithaca, NY, USA, June 1970.
- [51] J. H. Wood, "Earthquake-induced soil pressures on structures," Rep. EERL 73-05, Earthquake Engineering Research Laboratory, California Institute of Technology, Pasadena, CA, USA, 1973.
- [52] D.-D. Nguyen, D. Park, S. Shamsheer, V.-Q. Nguyen, and T.-H. Lee, "Seismic vulnerability assessment of rectangular cut-and-cover subway tunnels," *Tunnelling and Underground Space Technology*, vol. 86, pp. 247–261, 2019.
- [53] N. Wagner and N. Sitar, "Seismic earth pressure on basement walls with cohesionless backfill," Ph.D. dissertation, University of California, Berkeley, CA, USA, 2016.
- [54] A. Hushmand, S. Dashti, C. Davis et al., "Seismic performance of underground reservoir structures: insight from centrifuge modeling on the influence of backfill soil type and geometry," *Journal of Geotechnical and Geoenvironmental Engineering*, vol. 142, no. 11, article 04016058, 2016.



Hindawi

Submit your manuscripts at
www.hindawi.com

